NEUROSCIENCE

A drug pocket at the lipid bilayer–potassium channel interface

Nina E. Ottosson,[1] Malin Silverå Ejneby,[1]* Xiongyu Wu,[2]* Samira Yazdi,[3†] Peter Konradsson,[2] Erik Lindahl,[3,4] Fredrik Elinder[1‡]

Many pharmaceutical drugs against neurological and cardiovascular disorders exert their therapeutic effects by binding to specific sites on voltage-gated ion channels of neurons or cardiomyocytes. To date, all molecules targeting known ion channel sites bind to protein pockets that are mainly surrounded by water. We describe a lipid-protein drug-binding pocket of a potassium channel. We synthesized and electrophysiologically tested 125 derivatives, analogs, and related compounds to dehydroabietic acid. Functional data in combination with docking and molecular dynamics simulations mapped a binding site for small-molecule compounds at the interface between the lipid bilayer and the transmembrane segments S3 and S4 of the voltage-sensor domain. This fundamentally new binding site for small-molecule compounds paves the way for the design of new types of drugs against diseases caused by altered excitability.

INTRODUCTION

Several existing pharmaceutical drugs against epilepsy, cardiac arrhythmia, and pain bind to voltage-gated ion channels to alter their function, thereby reducing cellular excitability (*1*, *2*). Most of these drugs bind to the ion-conducting pore (a in Fig. 1A) to block ion flux (*3*, *4*). A few compounds bind to the gate (b in Fig. 1A) to bend it open (*5*, *6*) or to the top of the voltage-sensor domain (VSD; c in Fig. 1A) to alter the channel's voltage sensitivity (*7*–*9*). These drug-binding sites are defined mainly by protein surfaces and are surrounded by water. Only occasionally do these channel-bound drugs face the lipid bilayer. For instance, small-molecule aryl sulfonamides, blocking the voltage-gated sodium type 1.7 ($Na_V1.7$) channel, bind between the transmembrane segments S2, S3, and S4 at the center of the VSD, but a flexible tail of the molecule makes contact with a phospholipid (*7*). Another example is the adamantane compounds that bind to fenestrations of the voltage-gated potassium type 7.1 ($K_V7.1$) channel, but these fenestrations are only available when KCNE1 accessory subunits are bound to the channel (*10*).

However, other types of compounds use the lipid bilayer as the major interaction surface: (i) Site-2 and site-5 toxins are hydrophobic compounds, partly using the lipid membrane to exert their effects on Na_V channels (*11*, *12*). (ii) Spider toxins bind with high affinity and specificity to the VSD, facing the lipid bilayer, to alter ion channel gating (*13*, *14*). (iii) Hydrophobic and negatively charged polyunsaturated fatty acids (PUFAs; illustrated by the negative charge in Fig. 1A) are suggested to dwell in the lipid bilayer and interact with the VSD to electrostatically affect the positively charged voltage sensor (*15*–*18*). However, no small-molecule drug-like compound is known to use a major lipid-facing site.

Dehydroabietic acid (DHAA; Fig. 1B) and its derivatives, analogs, and related compounds open K_V and big-conductance Ca^{2+}-activated K (BK) channels (*16*, *19*–*21*). Halogenation of C12 and small nonpolar side chains on C7 (Fig. 1B) increase the capacity to open a K_V channel (*19*), but the sites of action are not known and might differ from channel to channel. Here, we searched for the site of interaction (referred to as the binding site throughout this paper) between the resin acids and a K_V channel. We report the first case of small molecules binding mainly to the lipid-exposed VSD surface, opening up the potential for design of new types of disease-curing small-molecule compounds.

RESULTS

Wu32 selectively slows down the closing transition

In total, we have synthesized and electrophysiologically explored 125 compounds (table S1) on the Shaker K_V channel expressed in *Xenopus laevis* oocytes. One hundred micromolar of one of the most potent DHAA derivatives, Wu32 (Fig. 1B), did not affect the opening kinetics of the wild-type (WT) Shaker K_V channel at +50 mV but slowed down the closing kinetics at −50 mV by a factor of 17.3 ± 2.3 (n = 5; Fig. 1C and fig. S1, A and B). Therefore, as a consequence, Wu32 kept the channel in an open state and, thereby, shifted the conductance-versus-voltage [$G(V)$] curve in the negative direction along the voltage axis (Fig. 1D). The $G(V)$ shift, measured at the 10% level of the maximum conductance in control solution (see Materials and Methods), was −14.7 ± 1.6 mV (n = 10). Two extra, positively charged, arginines at the extracellular end of the voltage sensor S4 [M356R/A359R; together with the wild-type residue R362 they form the active arginine triad, and hence it is called the 3R channel (*16*, *19*)] enhanced the Wu32-induced $G(V)$ shift to −30.0 ± 1.8 mV (n = 8; Fig. 1E), suggesting that the S4 of the VSD is the target for Wu32.

Furthermore, the 3R mutation enhanced the compound effect on the closing kinetics but had no effect on the opening kinetics at positive voltages (Fig. 1F and fig. S1C). These data are consistent with a model where Wu32 binds close to S4 in its activated up state (Fig. 1A) to prevent the downward movement of S4 and the closure of the channel (Fig. 1G). This model predicts a very slow opening at intermediate voltages, which was found experimentally (fig. S1D). Ion channels undergo multiple activation steps before channel opening (*22*–*24*). Studies on the ILT mutant (V369I/I372L/S376T)—which separates the early, major charge-carrying steps from the last channel-opening step (*25*)—showed that, although the gating currents (early steps) are not affected by Wu32, the $G(V)$ (last step) is shifted by −63.9 ± 3.1 mV

[1]Department of Clinical and Experimental Medicine, Linköping University, Linköping, Sweden. [2]Department of Physics, Chemistry and Biology, Linköping University, Linköping, Sweden. [3]Science for Life Laboratory, Department of Biochemistry and Biophysics, Stockholm University, Stockholm, Sweden. [4]Department of Physics, Swedish e-Science Research Centre, KTH Royal Institute of Technology, Stockholm, Sweden.
*These authors contributed equally to this work.
†Present address: Department of Clinical and Experimental Medicine, Linköping University, Linköping, Sweden.
‡Corresponding author. Email: fredrik.elinder@liu.se

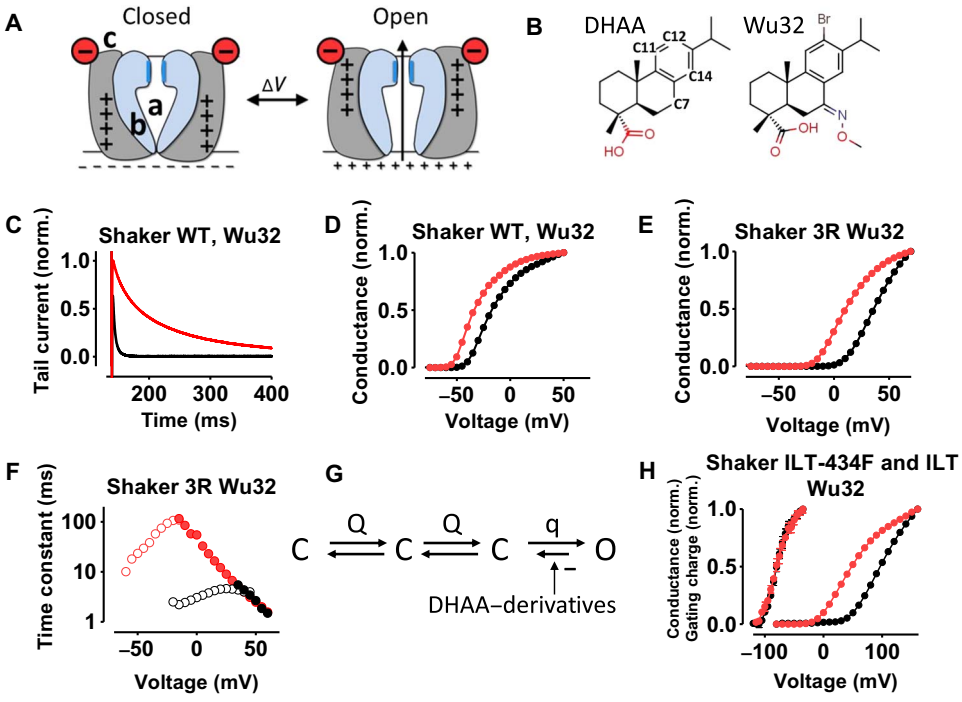

Fig. 1. Wu32 keeps the Shaker K_V channel in the open state. (**A**) Cartoons of a voltage-gated ion channel. a to c are principal drug-binding sites described in the text. Negatively charged polyunsaturated fatty acids (PUFAs) (in red) attract the gating charges to open the channel. (**B**) Molecules studied. (**C** to **F** and **H**) Channels as indicated: black, control; red, 100 μM Wu32 (pH = 7.4). Holding voltage (V_H) = −80 mV. (C) Representative normalized tail currents at −70 mV, following a step to +50 mV. (D) Representative $G(V)$ shift = −16 mV. (E) Representative $G(V)$ shift = −29 mV. (F) Time constants as indicated. Closed symbols measured from the opening and open symbols measured from the closing. (**G**) Kinetic scheme for the Shaker K_V channel. C, closed states; O, open state; Q, large gating change; q, small gating charge. (**H**) ILT-434F (curves to the left): No shift of gating currents [V_H = −100 mV; mean ± SEM (n = 3)]. ILT (curves to the right): $G(V)$ shift = −63.9 ± 3.1 mV (n = 5). Norm., normalized.

(n = 5; Fig. 1H). This suggests that Wu32 acts on the O→C transition (Fig. 1G and fig. S1, E to H).

To quantitatively evaluate the obtained data, we used a simple Shaker K_V channel model, which includes four independent and relatively steeply voltage-dependent steps, followed by a common, less voltage-dependent opening step of the channel (*15*). Imposing a closing step (O→C transition) that is 17.3 times slower predicts a voltage shift of the WT $G(V)$ curve by −12.9 mV (compared to −14.7 mV found experimentally), a voltage shift of the ILT $G(V)$ curve by −69.9 mV (compared to −63.9 mV found experimentally), and a voltage shift of the ILT $Q(V)$ by 0.0 mV (compared to no shift found experimentally). Thus, the experimental data fit exceedingly well with the hypothesis that only the first closing step is affected.

Mutated S3 residues alter the Wu32 effect

Because residues M356R and A359R of the lipid-facing extracellular end of S4 are important for the Wu32-induced $G(V)$ shift (Fig. 1, D to F), we hypothesized that Wu32 binds close to the extracellular end of S3 to alter the S4 movement, sterically or electrostatically. If so, then the effect of Wu32 should be sensitive to an introduced charge at the extracellular end of S3; a positive charge is expected to deprotonate and/or attract Wu32 to increase the effect, and a negative charge is expected to protonate and/or repel Wu32 to decrease the effect. To test this, we altered the charge of residue 325, which is close to the positive charges of S4 (*26*). The positively charged cysteine-specific reagent $MTSEA^+$ (2-aminoethyl methanethiosulfonate hydrochloride) significantly increased the Wu32-induced $G(V)$ shift of I325C (Fig. 2A), consistent with residue 325 being close to the binding pocket. The negatively charged cysteine-specific reagent $MTSES^-$ [sodium (2-sulfonatoethyl)methanethiosulfonate] significantly reduced the effect (Fig. 2A), as expected from an electrostatic effect. This suggests that Wu32 binds close to residue 325 in the top of S3.

If Wu32 binds close to the top of S3, then it is possible that some residues of S3 directly interact with Wu32. To explore this, we mutated all residues in the extracellular half of S3 to small and polar cysteines, which are not present in the WT. Five out of 15 tested mutations significantly altered (increased) the compound-induced $G(V)$ shift (Fig. 2B, in red). The increase in the $G(V)$ shift can be caused by either an increased affinity of the compound to the channel or an increased efficacy. However, because saturation of the dose-response curves was not reached in the concentration range that is possible to explore [up to 300 μM (*19*)], it has not been possible to unequivocally decide on efficacy versus affinity. The increase in effect suggests that the cysteine mutations either (i) structurally alter the binding pocket to indirectly alter the affinity and/or efficacy or (ii) alter hydrogen bonding to directly alter the affinity and/or efficacy of Wu32. Three of these residues (I318C, P322C, and T326C) point toward S4 (Fig. 2C), whereas two residues (I320C and F324C) point toward S2. Residue 325, used for the electrostatic investigation above, is located between the two clusters, pointing toward the lipid bilayer (Fig. 2C). Thus, it is possible that Wu32 binds in the S2/S3 cleft, the S3/S4 cleft, or in both.

The largest mutation effect was found for P322C, possibly depending on a major alteration in S3. The proline in S3 is rather conserved among K_V channels (*12*) and makes S3 bend (*27*, *28*). We hypothesize that the P322C mutation straightens S3 to better accommodate Wu32 in a pocket. If residue 322 directly points toward the binding site for

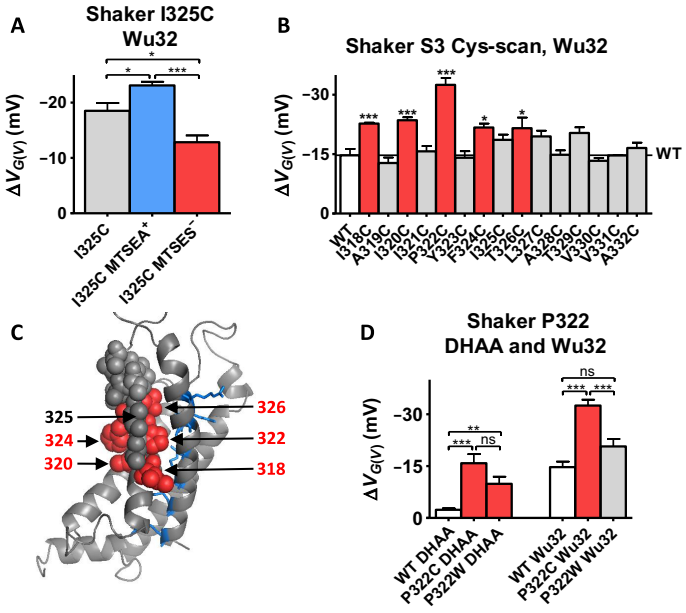

Fig. 2. Effects of S3 mutations on compound-induced *G*(*V*) shifts. (**A**) Effects on I325C (gray bar) and modifications of the positively charged $MTSEA^+$ (red bar) and the negatively charged $MTSES^-$ (blue bar), respectively. Data are means ± SEM (n = 4 to 5). *P < 0.05; ***P < 0.001 [one-way analysis of variance (ANOVA) together with Bonferroni's multiple comparison test]. (**B**) $G(V)$ shifts of 100 μM Wu32 (pH 7.4) on S3 mutations. Data are means ± SEM (n = 4 to 10). $G(V)$ shifts are compared with WT (white bar, black line): gray bars, not different from WT; red bars, significantly different from WT. *P < 0.05, **P < 0.01, ***P < 0.001(one-way ANOVA together with Dunnett's multiple comparison test). (**C**) Mutated residues as space filled in one VSD of the Shaker K_V channel in the open state (side view) (*23*). Gating charges, blue sticks. Color coding as in (B). (**D**) Effects of P322 mutations on DHAA- and Wu32-induced $G(V)$ shifts as indicated. Data are means ± SEM (n = 4 to 10). Color coding as in (B). *P < 0.05, ***P < 0.001(one-way ANOVA together with Bonferroni's multiple comparison test). ns, not significant.

Wu32, then a bulkier residue (making the pocket shallower) is expected to decrease the effect. The P322W mutation, which is bulkier, reduced the $G(V)$ shift of Wu32 (Fig. 2D). Thus, the S3 mutations are consistent with Wu32 binding in a pocket between S3 and S4, but the alternative site between S2 and S3 has not been refuted so far.

There are electrostatic interactions between the resin acid and S4

The effects described above can be explained by a state-dependent binding to the open state. However, it is also clear that the charge of the compound is critical for the effect; the DHAA derivative–induced $G(V)$ shifts are pH-dependent (Fig. 3A and fig. S2), suggesting that a fully charged molecule is needed for maximum effect; an uncharged molecule lacks effect. This is supported by the finding that a permanently charged DHAA analog (Wu164) at pH 7.4 shifts the $G(V)$ equally as much as DHAA at pH 9 and 10 (fig. S2, A and B). A central question is whether the charge is critical for the binding (affinity) or for the effect (efficacy) of the $G(V)$ shift. If there is an electrostatic interaction causing the effect, then a positive charge should have the opposite effect; a Wu32-amine (Wu165; Fig. 3B) pH-dependently shifted the $G(V)$ in a positive direction along the voltage axis (Fig. 3A), thus supporting an electrostatic effect.

Because there is an electrostatic interaction between the DHAA derivative and S4, an alteration of the charge structure of the extracellular end of S4 should affect the $G(V)$ shift in a systematic way. To explore this, we inserted a positively charged arginine in the positions 356 to 362, one by one, in the background of R362Q (a channel with no charge between residues 356 and 364). Wu32 shifted the $G(V)$ of R362Q by −32.0 ± 2.0 mV (n = 8; Fig. 3C). For the WT and 3R Shaker K_V channels, the closing kinetics, but not the opening kinetics, of R362Q were affected by Wu32 (fig. S3). Arginines in positions 359 or 360 increased the absolute shift, whereas arginines in positions 357, 361, or 362 decreased the shift (Fig. 3D). A simple model could explain these effects if electrostatic attractions between Wu32 and an arginine at positions 359 or 360 rotate S4 clockwise to open the channel (*16*), whereas attractions between Wu32 and arginines in positions 357, 361, or 362 rotate S4 counterclockwise to close the channel (Fig. 3, E to F). The direction of this rotation is consistent with what has been reported before (*23*, *29*). An arginine at position 356 (M356R/R362Q) did not change the effect of Wu32 compared to R362Q (Fig. 3D), probably because 356 is reaching out into the extracellular water and is screened by extracellular ions. To further test these electrostatic interactions, we altered the charge for the most sensitive positions (359, 360, and 361) to negatively charged glutamates. As expected, a glutamate in positions 359 or 360 decreased the Wu32-induced $G(V)$ shift, and a glutamate in position 361 increased the Wu32-induced $G(V)$ shift (Fig. 3G). For the S4 mutants, there was a close correlation between the effects of Wu32 and DHAA (Fig. 3H), suggesting a common binding site, but Wu32 is six times more efficient. An interesting implication of the data presented here is that channels lacking R1 (=R362) might be more sensitive to DHAA derivatives and analogs. The electrostatic data strongly support a binding site for DHAA and Wu32 in the S3/S4 cleft (Fig. 3F) while refuting a binding site in the S2/S3 cleft.

Resin acids act quantitatively different on kinetics

Whereas Wu32 had a very large effect on the closing kinetics (Fig. 1, C and F), the effect of DHAA was much smaller despite shifting the $G(V)$ curve substantially along the voltage axis (Fig. 4A). DHAA behaves as if it exerts a pure electrostatic effect with no additional effects on gating. This is similar to what has been described for PUFAs (*15*, *16*, *30*). If the $G(V)$ curve is shifted by −12 mV, then the corresponding time constant–versus–voltage curve (Fig. 4B) is also expected to be shifted by −12 mV along the voltage axis. This means that the opening kinetics is slightly speeded up (by a factor of 1.5 to 2) and that the closing kinetics is slightly slowed down (also by a factor of 1.5 to 2; Fig. 4, A and B). We envision that Wu32, possibly because of its methyloxime group (Fig. 1B), has a deeper and tighter binding to the S3/S4 cleft than DHAA, with an additional allosteric effect on the closing kinetics. To find a DHAA derivative with an even tighter binding to the channel suitable for molecular docking, we therefore searched for a compound with a large effect on the closing kinetics. All compounds with $G(V)$ shifts larger than |−20| mV (table S1) were investigated for their effects on the closing kinetics; some compounds deviated from the predicted electrostatic effects (Fig. 4C, black line, and fig. S4), suggesting an additional allosteric effect. The compound with the largest effect on the closing kinetics was Wu122 with a methyloxime group at C7 and a cyclopropyl group at C12 (Fig. 4D).

Molecular docking supports the S3/S4 cleft as binding site

Both the experimental data above and previous simulations of PUFAs point to a tentative binding pocket in the cleft between S3 and S4 (*17*). An initial 500-ns molecular dynamics simulation of the Shaker WT in a membrane with several Wu122 molecules placed outside the subunits

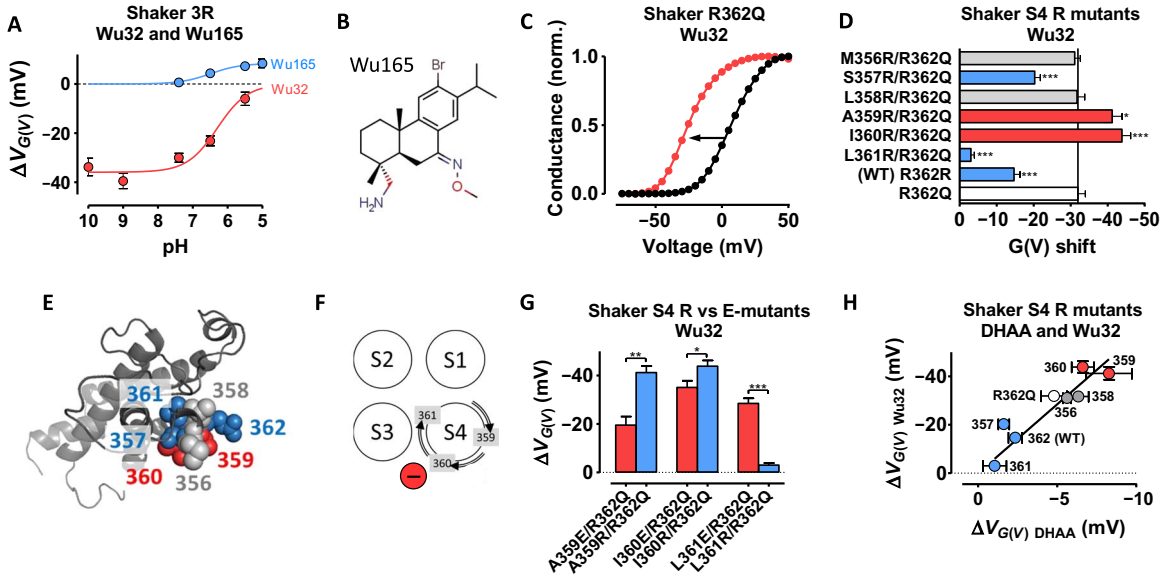

Fig. 3. Electrostatic interactions between S4 and the DHAA derivatives. All compounds 100 μM (pH 7.4 if not otherwise stated). (**A**) pH dependence for $G(V)$ shifts. Data are means ± SEM (n = 4 to 8). (**B**) Molecular structure of the amine (Wu165) in (A). (**C**) Black, control; red, Wu32. $G(V)$ shift = −33 mV. (**D**) Wu32-induced $G(V)$ shifts for arginine mutants. Data are means ± SEM (n = 4 to 10). $G(V)$ shifts are compared with R362Q (white bar, black line): gray bars, not different from R362Q; blue bars, significantly smaller than R362Q; red bars, significantly larger than R362Q. *P < 0.05, ***P < 0.001 (one-way ANOVA together with Dunnett's multiple comparison test). (**E**) Mutated residues as space fill in one VSD of the Shaker K_V channel in the open state. Coloring as in (D). (**F**) Schematic illustration of S4 rotation during last (opening) step. The red symbol denotes a position consistent with data. (**G**) Effects of glutamate mutations (red bars) on Wu32-induced shifts, compared to arginine mutations (blue bars) from (D). Data are means ± SEM (n = 4 to 6). *P < 0.05, **P < 0.01, ***P < 0.001(t test). (**H**) Wu32-induced $G(V)$ shifts from (D) versus DHAA-induced $G(V)$ shifts. Data are means ± SEM (n = 4 to 10), slope = 5.7. Wu32 data in (A), WT data in (D) and (H) from the study of Ottosson *et al*. (*19*).

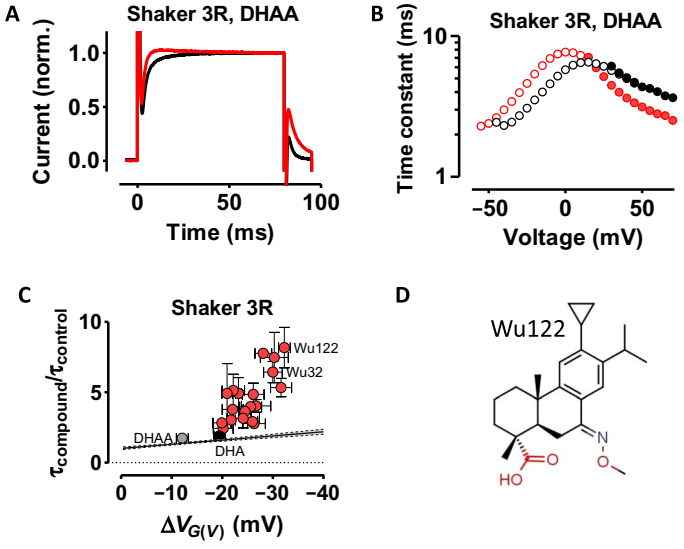

Fig. 4. Resin acid effects on kinetics. (**A** and **B**) Effects on opening and closing kinetics of the 3R Shaker K_V channel. Black, control; red, 100 μM DHAA (pH 7.4). (A) Normalized currents. Opening at +40 mV (0 to 80 ms) and closing at −20 mV (80 to 95 ms). (B) Effects on time constants. Closed symbols measured from the opening and open symbols measured from the closing. (**C**) Relative closing time constants ($\tau_{compound}/\tau_{control}$) at −20 mV, following 100 ms at +70 mV. Black line, linear regression from fig. S5. Dashed lines, confidence interval. Red symbols, DHAA derivatives with $G(V)$ shift >|−20| mV. Date are means ± SEM (n = 4 to 11). (**D**) Molecular structure of Wu122.

confirmed this, with two-thirds of all residue interactions and all high-probability interactions occurring in the S3/S4 cleft (fig. S5, A and B). Because all results point to the S3/S4 region, a docking grid was selected to cover three sites along the vertical axis of the S3/S4 cleft of the WT Shaker K_V channel. This does not include intersubunit locations, and hence, it was sufficient to use a single VSD for the docking. The poses with the highest predicted scores differed in the preferred orientation of Wu122 relative to the channel (fig. S5C). The results were further evaluated by subjecting the Shaker-Wu122 complexes to molecular dynamics simulations to assess the ability of each structure to maintain its predicted pose. In all simulations, Wu122 moved to orientations similar to one of the docked poses with the compound accommodating itself near the S3-S4 linker, with the charged carboxylic group steered toward the S3/S4 cleft and the important C7 side chain (*19*) pointing into the hydrophobic core of this region (Fig. 5, A to C, and fig. S5D). Although there are significant fluctuations of the S3-S4 linker, the S3/S4 segments stay quite stable during relaxation, with only a slight widening of the cleft with Wu122 bound (fig. S6, A and B). In particular, I318 and T326 are partly accessible to the lipid environment, with only minor changes related to Wu122 binding (fig. S6C).

The poses of Wu122 with the charged group buried in the membrane changed early in the simulations, with the compound reorienting itself and floating up like a cork to the surface. This explains why podocarpic acid (an analog of DHAA) with a polar hydroxyl group at C12 did not have any effect on the Shaker K_V channel (*19*). In terms of the interactions between the channel and the Wu122 compound, a number of electrostatic networks mediated by sodium ions appear to involve acidic residues (E333, E334, E335, and D336) located on the

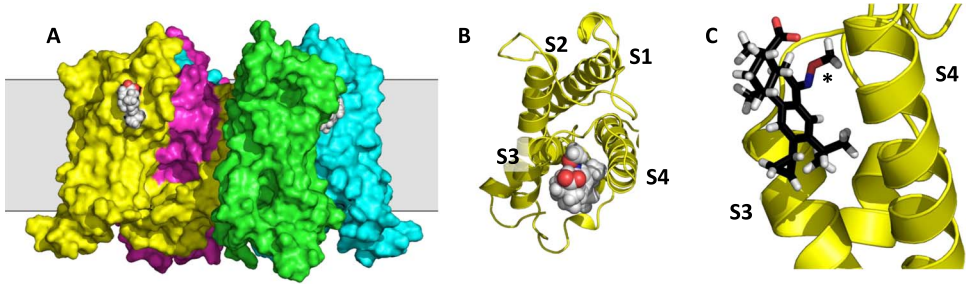

Fig. 5. Molecular dynamics identifies an interaction site between S3, S4, and the lipid bilayer. (**A**) Predicted binding pose of Wu122 on the WT Shaker K_V channel. Different colors denote different subunits. (**B**) Top view and (**C**) side view of one VSD. *, C7 side chain.

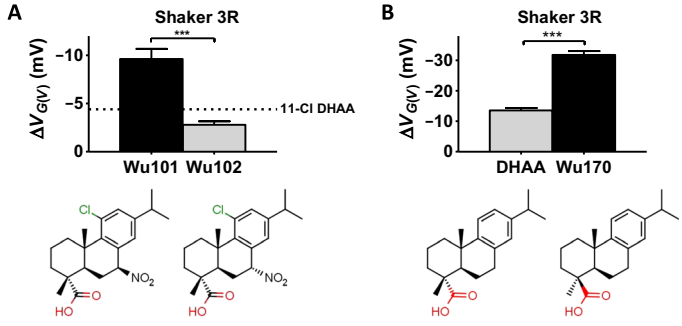

Fig. 6. Small side chain alterations have large effects compound-induced *G*(*V*) shifts. (**A** and **B**) *G*(*V*) shifts for 100 μM compound (pH 7.4). (A) Effect of chirality in the nitro group. Dashed line, molecule lacking the nitro group (*19*). Data are means ± SEM (n = 5 to 6). ***P < 0.0001 (*t* test). (B) Effects of chirality of the carboxyl group. Data for DHAA (*19*). Data are means ± SEM (n = 4 to 11). ***P < 0.0001 (*t* test).

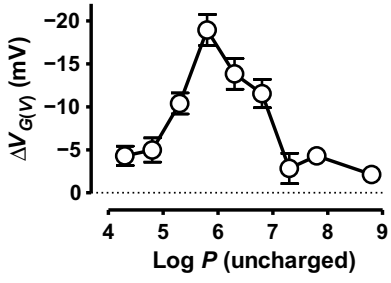

Fig. 7. Log *P* values for all compounds. *G*(*V*) shifts at a concentration of 100 μM and pH 7.4 versus calculated log *P* values for all tested 125 compounds (bin size = 0.5; table S1).

S3-S4 linker mediated by the sodium ions in the system, and a few hydrogen bonds formed with residues T329, S351, Q354, and S357 (fig. S5B). However, attempts to break some of the bonds did not reduce the compound-induced *G*(*V*) shift (fig. S7), suggesting that multiple interactions are formed or that the loss of negatively charged residues might be compensated by electrostatic interactions with lipid head groups.

Side chain differences of the resin acids alter function

If the DHAA derivatives fits well in the S3/S4 cleft, then the compound-induced *G*(*V*) shift should be sensitive to small structural alterations around C7. Chirality alterations of a nitro group at C7 induced a large difference in the compound-induced *G*(*V*) shift (Fig. 6A). In addition, the different chirality of the carboxyl group had a large effect (Fig. 6B). The increased *G*(*V*)-shifting property of Wu170 compared to DHAA (Fig. 6B) parallels an increased slowing of the closing kinetics (fig. S8). Thus, the chirality of the carboxyl group of Wu170 is a key factor to increase the effect of DHAA derivatives to stabilize the K channel in the open state.

DISCUSSION

In summary, we have identified small molecules binding to a new lipid-facing pocket in a K_V channel, formed by S3 and the sliding voltage sensor S4, and modulating channel function. The overall data also suggest some general properties of potent compounds; there is a strong correlation between log *P* and the compound-induced *G*(*V*) shift (Fig. 7 and fig. S9A), with a sharp peak around log P = 6. For all but one of the 20 best shifters [>|−20| mV, 100 μM (pH 7.4), 3R channel], the log *P* values were 5.5 to 6.5. These large values support binding to the lipid bilayer. This interaction with the lipid bilayer also suggests that these compounds will find its way to the pocket faster by exploiting the so-called reduction-in-dimensionality principle (*31*). The calculated pK_a (where K_a is the acid dissociation constant) values (in water) are more widely distributed, but all the 20 best shifters have pK_a values below 4.5 (fig. S9B and table S1). This suggests that compounds with a high-shift propensity should have a moderate degree of hydrophobicity (log $P \approx 6$) and a high degree of deprotonated carboxyl groups (pK_a < 4.5).

Several mutations of the channel (for instance, P322C, R362Q, and A359R) all largely increase the effect of the compounds, and many alterations of the mother compound DHAA (chirality of the carboxyl group, chirality of C7, side chain of C7, halogenation of the C11-14, and alteration of side chains at C12 or C13) markedly increase the effect. These findings suggest that it is possible to specifically design compounds acting on specific ion channels with high affinity and specificity to alter ion channel gating and serving as pharmaceutical compounds against several diseases.

MATERIALS AND METHODS

Molecular biology and expression of ion channels

The Shaker H4 channel (*32*), with removed N-type inactivation (ShH4IR) (*33*), is called the WT Shaker K_V channel. The conducting ILT mutant (V369I/I372L/S376T) (*25*) and the nonconducting ILT mutant (referred to as 434-ILT; C245V/V369I/I372L/S376T/C426A/W434F) were provided by E. Isacoff (University of California, Berkeley, Berkeley, CA). Mutagenesis, complementary RNA injection, and oocyte storage were performed according to the procedures described previously (*15*, *16*, *19*, *34*). All animal experiments were approved by the Linköping's local Animal Care and Use Committee, and the experiments were performed in accordance with relevant guidelines and regulations.

Electrophysiology

Currents were measured with the two-electrode voltage-clamp technique (GeneClamp 500B amplifier, Digidata 1440A digitizer, and pClamp 10 software; Molecular Devices) 1 to 6 days after injection of RNA. The amplifier's leak and capacitance compensation were used, and currents were low-pass–filtered at 5 kHz. All experiments were performed at room temperature (20° to 23°C). The holding voltage was set to −80 mV (−120 mV for the L361R/R362Q mutant), and steady-state currents were achieved by stepping to voltages between −80 and +50 mV (adjusted for some of the mutants) for 100 ms in 5-mV increments (between −80 and +160 mV for 300 ms in 10-mV increments for the ILT channel). The activation pulse was followed by a pulse (−20 mV; adjusted for some of the mutants) to analyze closing kinetics. OFF gating currents of 434-ILT mutant were measured by first stepping to −120 mV for 100 ms, then to prepulse voltages between −120 mV and +10 mV in 5-mV increments, and finally to −100 mV for 200 ms. Capacitance compensation for the gating current measurements was carried out from a holding voltage of 0 mV.

The control solution contained 88 mM NaCl, 1 mM KCl, 15 mM Hepes, 0.4 mM $CaCl_2$, and 0.8 mM $MgCl_2$. pH was adjusted to 7.4 with NaOH, yielding a final sodium concentration of about 100 mM. Control solution was added using a gravity-driven perfusion system. Compounds (DHAA and its derivatives and analogs) were initially dissolved in 100 mM dimethyl sulfoxide and stored at −20°C and were subsequently diluted to the desired test concentration in control solution. The compound solution was added to the bath using a syringe.

Analysis of electrophysiological data

The electrophysiological data were processed and analyzed by Clampfit 10.5 (Molecular Devices) and GraphPad Prism 5 (GraphPad Software).

Estimation of the G(V) shift

The conductance $G(V)$ was calculated as

$$G(V) = I/(V - V_{rev}) \quad (1)$$

where I is the average current from the steady-state phase at the end of each pulse (100 or 200 ms after onset of pulse), V is the absolute membrane voltage, and V_{rev} is the reversal potential for the K_V channel (set to −80 mV). Equation 1 assumes that the current through an open K_V channel follows Ohm's law. This is not always true. Instead, in some preparations, the current through an open K_V channel follows the constant-field equation (*35*) or, as it is also called, the Goldman-Hodgkin-Katz (GHK) equation (*36*). However, whether we use Eq. 1 or the GHK equation does not affect the conclusion. Simulation of data shows that the error depending on the choice of analysis is at most 1% (fig. S10).

These data were fitted to a Boltzmann equation

$$G(V) = A/\left(1 + \exp\left(\left(V_{1/2} - V\right)/s\right)\right)^n \quad (2)$$

where A is the amplitude of the curve, V is the absolute membrane voltage, $V_{½}$ is the midpoint, s is the slope, and n is an exponent set to 4 (*30*).

The most marked effects of the DHAA derivatives and analogs investigated in the present study were negative shifts of the $G(V)$ curve along the voltage axis. If there is no alteration in slope or amplitude, as sometimes reported for PUFAs (*37*), then the shift can be measured at any level of the $G(V)$ curve, always giving the same results. However, for some compounds and mutated channels, the effect cannot be described by a simple translation of the $G(V)$ curve; there is a combination of an amplitude increase and a shift of the $G(V)$ curve (*16*, *19*). The shift of the $G(V)$ curve can either be determined (i) by calculating the difference between $V_{½}$ in control solution and $V_{½}$ in compound solution or (ii) by determining the shift at the foot of the curve without a normalization of the curve (*30*). Because our focus was to find, explore, and design compounds altering excitability, the shift of the foot of the $G(V)$ curve is most important (*30*), and therefore, we have measured the $G(V)$ shift at the 10% level of the maximum conductance in control solution (*30*). Furthermore, in some cases, the 10% method (ii) is more accurate than the $V_{½}$ method (i) (fig. S10).

However, although there is a substantial alteration in the amplitude of the curve, the 10% method is insensitive to this alteration. The "error," depending on what we mean by correct estimation, at the 10% level compared to the alteration in $V_{½}$ can be derived from Eq. 2 (for derivation, see Supplementary Methods)

$$\Delta V_{error} = s\left[\ln\left((10)^{1/n} - 1\right) - \ln\left(\left((10)(A_{cmpd}/A_{cntrl})\right)^{1/n} - 1\right)\right] \quad (3)$$

A_{cmpd}/A_{cntrl} is the relative effect on G_{max} by the compound. If $s = 6$ mV, $n = 4$, and the amplitude is less than doubled ($A_{cmpd}/A_{cntrl} = 2$), then the error is less than 2.2 mV. Because the amplitude increment is smaller, the error is negligible, and thus, we used the 10% level to determine the shift.

Estimation of the Q(V) shift

$Q(V)$ was analyzed by integrating the OFF gating current before and after compound application. The gating charge was normalized (relative to current at −30 mV) and plotted against the prepulse voltage.

Estimation of time constants

The time constant τ for closing kinetics for short closure pulses (20 ms) was calculated from a single exponential function

$$I(t) = (A_1 * e\wedge(-t/\tau_1)) + C \quad (4)$$

where A_1 is the amplitude, τ_1 is the time constants, t is the time, and C is a constant. The fit was performed by using Clampfit 10.5 (Levenberg-Marquardt search method; precision, 10^{-6} with a maximum of 5000 iterations). In some cases, we used longer pulses and fitted a double exponential function

$$I(t) = (A_1 * e\wedge(-t/\tau_1)) + (A_2 * e\wedge(-t/\tau_2)) + C \quad (5)$$

where A_1 and A_2 are amplitudes, τ_1 and τ_2 are time constants, t is the time, and C is a constant. A weighted τ value was calculated

$$\tau_{weighted} = \left((A_1 * \tau_1) + (A_2 * \tau_2)\right)/(A_1 + A_2) \quad (6)$$

The error was calculated according to the propagation of error according to the variance formula.

Chemical properties of the compounds

To draw chemical structures and to calculate pK_a and log P values, we used Marvin [Marvin Suite 16.12.9, 2016, ChemAxon (http://chemaxon.com)]. pK_a values for the acids were calculated using

Calculation Plugin (mode, macro; acid/base prefix, dynamic; minimum basic pK_a, −5; maximum acidic pK_a, 12; temperature, 298 K; correction library, used). Log *P* values were calculated using Calculation Plugin (method, consensus; electrolyte concentrations, 0.1 mol/dm^3).

Docking protocol

An open-state model of the WT Shaker K_V channel was built from the K_V1.2/2.1 chimera (Protein Data Bank 2R9R) (*27*) and relaxed in a pure phosphatidylcholine (POPC) bilayer with parameters and setup as previously described (*17*). The most potent compound, Wu122, was used for the docking study. A single subunit was used for docking, removing water, ions, and lipids present in the simulation. Aspartic acid, glutamic acid, arginine, and lysine residues had protonation states corresponding to pH 7, whereas histidine residues were neutral with protonation determined by the local hydrogen bonding network.

Docking was performed with DOCK 3.6 (*38*), using a flexible ligand-sampling algorithm to overlay docked molecules onto binding-site matching spheres. The coordinates of a Shaker-bound PUFA in a proposed interaction site from previous work (*17*) was selected as a reference for the binding site. To improve the exploration of the interaction site, we separated the cleft into three distinct putative binding sites at different vertical positions. This allowed a total of 120 matching spheres to distinguish each binding site. The spheres were also labeled for chemical matching based on the local receptor environment (*39*). Bin size, overlap, and distance tolerance were set to 0.3, 0.1, and 1.4 Å, respectively (for both the matching spheres and the docked molecules). A physics-based scoring function was used for the ligand conformations that had passed the initial steric filter. The highest-scoring conformation of each docked molecule was subjected to 100 steps of rigid-body minimization. The score for each conformation was calculated as the sum of the receptor-ligand electrostatic and van der Waals interaction energy, corrected for ligand desolvation (evaluated from precalculated grids). The three-dimensional map of the electrostatic potential in the binding site was prepared using the program Delphi (*40*) and partial charges from the united-atom AMBER force field (*41*). ChemGrid was used to generate a van der Waals grid (*42*). The desolvation penalty for a ligand conformation was estimated from transfer-free energy of the molecule between solvents of dielectric constants 78 and 2. The ligand was assumed to completely desolvate upon binding. The compound, Wu122, was prepared for docking by using the ZINC database protocol (*43*). Wu122 was docked to the Shaker model in three distinct vertical positions, and three top-ranked docked poses based on their predicted energy scores were selected.

Molecular dynamics simulation protocol

To initially assess the Shaker regions where Wu122 might interact and investigate a preferred binding mode and define the binding pocket, we subjected complete Shaker tetramers with Wu122 either placed outside each subunit or docked to the VSD to molecular dynamics simulations in a POPC bilayer (*17*). To enhance sampling of preferred channel-ligand poses, each Wu122 pose was copied to all subunits of the channel. For the docked poses, this resulted in three different systems, with each system containing a tetrameric Shaker K_V channel and four Wu122 molecules in different positions along the vertical axis of the S3-S4 cavity, surrounded by 430 POPC lipids and roughly 36,000 TIP3P waters. Each system was neutralized with 0.1 M NaCl. The systems were first relaxed with restraint applied to the Wu122 molecules for 100 ns, followed by an additional 100 ns where the position restraints on the Wu122 molecules were applied to the *z* coordinates only. Finally, all restraints were removed, and the systems were simulated for 200 ns. Force field parameters for the Wu122 compound were obtained from the multipurpose atom-typer for CHARMM (Chemistry at HARvard Macromolecular Mechanics; MATCH) server (*44*), which uses libraries of topology and parameter files in existing force fields for extrapolation to the new molecules consistent with the parameterization strategy within a given force field. The default CHARMM General Forcefield (top_all36_cgenff) was used for partial charges and parameterization. Simulations were performed using a development version of GROMACS (*45*, *46*) using 2-fs time steps and settings as previously reported (*17*).

Compound synthesis

The complete description of compound synthesis is found in Supplementary Methods.

Statistical analysis

Average values are expressed as means ± SEM. When comparing two compound-induced shifts, a two-tailed unpaired *t* test was used. When comparing compound-induced shifts with control, one-way ANOVA together with Dunnett's multiple comparison test was used. When comparing groups, one-way ANOVA together with Bonferroni's multiple comparison tests was used. Correlation analysis was done by Pearson's correlation test and linear regression. $P < 0.05$ is considered significant for all tests.

SUPPLEMENTARY MATERIALS

Supplementary material for this article is available at http://advances.sciencemag.org/cgi/content/full/3/10/e1701099/DC1

Supplementary Methods

fig. S1. Wu32 affects the closure step.

fig. S2. The charge of the resin acid is required for *G*(*V*) shifting effects.

fig. S3. Wu32 affects closure but not opening.

fig. S4. Small effects of DHA and DHAA on kinetics.

fig. S5. Molecular dynamics identifies an interaction site between S3, S4, and the lipid bilayer.

fig. S6. Stability of VSD-Wu122 complexes.

fig. S7. The negatively charged cluster EEED333-336 is not important for compound-induced *G*(*V*) shifts.

fig. S8. Wu170 affects closing but not opening.

fig. S9. Correlation analysis for 3R Shaker K_V channel.

fig. S10. The method to calculate conductance (or permeability) does not affect the estimated *G*(*V*) shift.

table S1. Properties of synthesized compounds.

References (*47*–*51*)

REFERENCES AND NOTES

1. G. W. Zamponi, J. Striessnig, A. Koschak, A. C. Dolphin, The physiology, pathology, and pharmacology of voltage-gated calcium channels and their future therapeutic potential. *Pharmacol. Rev.* **67**, 821–870 (2015).
2. W. A. Catterall, Sodium channels, inherited epilepsy, and antiepileptic drugs. *Annu. Rev. Pharmacol. Toxicol.* **54**, 317–338 (2014).
3. B. Hille, Local anesthetics: Hydrophilic and hydrophobic pathways for the drug-receptor reaction. *J. Gen. Physiol.* **69**, 497–515 (1977).
4. D. S. Ragsdale, J. C. McPhee, T. Scheuer, W. A. Catterall, Molecular determinants of state-dependent block of Na^+ channels by local anesthetics. *Science* **265**, 1724–1728 (1994).
5. T. V. Wuttke, G. Seebohm, S. Bail, S. Maljevic, H. Lerche, The new anticonvulsant retigabine favors voltage-dependent opening of the K_v7.2 (*KCNQ2*) channel by binding to its activation gate. *Mol. Pharmacol.* **67**, 1009–1017 (2005).
6. S. Marzian, P. J. Stansfeld, M. Rapedius, S. Rinné, E. Nematian-Ardestani, J. L. Abbruzzese, K. Steinmeyer, M. S. P. Sansom, M. C. Sanguinetti, T. Baukrowitz, N. Decher, Side pockets provide the basis for a new mechanism of Kv channel–specific inhibition. *Nat. Chem. Biol.* **9**, 507–513 (2013).

7. S. Ahuja, S. Mukund, L. Deng, K. Khakh, E. Chang, H. Ho, S. Shriver, C. Young, S. Lin, J. P. Johnson Jr., P. Wu, J. Li, M. Coons, C. Tam, B. Brillantes, H. Sampang, K. Mortara, K. K. Bowman, K. R. Clark, A. Estevez, Z. Xie, H. Verschoof, M. Grimwood, C. Dehnhardt, J.-C. Andrez, T. Focken, D. P. Sutherlin, B. S. Safina, M. A. Starovasnik, D. F. Ortwine, Y. Franke, C. J. Cohen, D. H. Hackos, C. M. Koth, J. Payandeh, Structural basis of Nav1.7 inhibition by an isoform-selective small-molecule antagonist. *Science* **350**, aac5464 (2015).
8. A. Peretz, L. Pell, Y. Gofman, Y. Haitin, L. Shamgar, E. Patrich, P. Kornilov, O. Gourgy-Hacohen, N. Ben-Tal, B. Attali, Targeting the voltage sensor of Kv7.2 voltage-gated K^+ channels with a new gating-modifier. *Proc. Natl. Acad. Sci. U.S.A.* **107**, 15637–15642 (2010).
9. P. Li, Z. Chen, H. Xu, H. Sun, H. Li, H. Liu, H. Yang, Z. Gao, H. Jiang, M. Li, The gating charge pathway of an epilepsy-associated potassium channel accommodates chemical ligands. *Cell Res.* **23**, 1106–1118 (2013).
10. E. Wrobel, I. Rothenberg, C. Krisp, F. Hundt, B. Fraenzel, K. Eckey, J. T. M. Linders, D. J. Gallacher, R. Towart, L. Pott, M. Pusch, T. Yang, D. M. Roden, H. T. Kurata, E. Schulze-Bahr, N. Strutz-Seebohm, D. Wolters, G. Seebohm, KCNE1 induces fenestration in the Kv7.1/KCNE1 channel complex that allows for highly specific pharmacological targeting. *Nat. Commun.* **7**, 12795 (2016).
11. W. A. Catterall, S. Cestèle, V. Yarov-Yarovoy, F. H. Yu, K. Konoki, T. Scheuer, Voltage-gated ion channels and gating modifier toxins. *Toxicon* **49**, 124–141 (2007).
12. S. I. Börjesson, F. Elinder, Structure, function, and modification of the voltage sensor in voltage-gated ion channels. *Cell Biochem. Biophys.* **52**, 149–174 (2008).
13. K. J. Swartz, Tarantula toxins interacting with voltage sensors in potassium channels. *Toxicon* **49**, 213–230 (2007).
14. K. J. Swartz, R. MacKinnon, Hanatoxin modifies the gating of a voltage-dependent K^+ channel through multiple binding sites. *Neuron* **18**, 665–673 (1997).
15. S. I. Börjesson, F. Elinder, An electrostatic potassium channel opener targeting the final voltage sensor transition. *J. Gen. Physiol.* **137**, 563–577 (2011).
16. N. E. Ottosson, S. I. Liin, F. Elinder, Drug-induced ion channel opening tuned by the voltage sensor charge profile. *J. Gen. Physiol.* **143**, 173–182 (2014).
17. S. Yazdi, M. Stein, F. Elinder, M. Andersson, E. Lindahl, The molecular basis of polyunsaturated fatty acid interactions with the Shaker voltage-gated potassium channel. *PLOS Comput. Biol.* **12**, e1004704 (2016).
18. F. Elinder, S. I. Liin, Actions and mechanisms of polyunsaturated fatty acids on voltage-gated ion channels. *Front Physiol.* **8**, 43 (2017).
19. N. E. Ottosson, X. Wu, A. Nolting, U. Karlsson, P.-E. Lund, K. Ruda, S. Svensson, P. Konradsson, F. Elinder, Resin-acid derivatives as potent electrostatic openers of voltage-gated K channels and suppressors of neuronal excitability. *Sci. Rep.* **5**, 13278 (2015).
20. Y.-M. Cui, E. Yasutomi, Y. Otani, K. Ido, T. Yoshinaga, K. Sawada, T. Ohwada, Design, synthesis, and characterization of BK channel openers based on oximation of abietane diterpene derivatives. *Bioorg. Med. Chem.* **18**, 8642–8659 (2010).
21. K. Sakamoto, Y. Suzuki, H. Yamamura, S. Ohya, K. Muraki, Y. Imaizumi, Molecular mechanisms underlying pimaric acid-induced modulation of voltage-gated K^+ channels. *J. Pharmacol. Sci.* **133**, 223–231 (2017).
22. L. Delemotte, M. Tarek, M. L. Klein, C. Amaral, W. Treptow, Intermediate states of the Kv1.2 voltage sensor from atomistic molecular dynamics simulations. *Proc. Natl. Acad. Sci. U.S.A.* **108**, 6109–6114 (2011).
23. U. Henrion, J. Renhorn, S. I. Börjesson, E. M. Nelson, C. S. Schwaiger, P. Bjelkmar, B. Wallner, E. Lindahl, F. Elinder, Tracking a complete voltage-sensor cycle with metal-ion bridges. *Proc. Natl. Acad. Sci. U.S.A.* **109**, 8552–8557 (2012).
24. W. N. Zagotta, T. Hoshi, R. W. Aldrich, Shaker potassium channel gating. III: Evaluation of kinetic models for activation. *J. Gen. Physiol.* **103**, 321–362 (1994).
25. C. J. Smith-Maxwell, J. L. Ledwell, R. W. Aldrich, Uncharged S4 residues and cooperativity in voltage-dependent potassium channel activation. *J. Gen. Physiol.* **111**, 421–439 (1998).
26. A. Broomand, F. Elinder, Large-scale movement within the voltage-sensor paddle of a potassium channel—Support for a helical-screw motion. *Neuron* **59**, 770–777 (2008).
27. S. B. Long, X. Tao, E. B. Campbell, R. MacKinnon, Atomic structure of a voltage-dependent K^+ channel in a lipid membrane-like environment. *Nature* **450**, 376–382 (2007).
28. Y. Li-Smerin, D. H. Hackos, K. J. Swartz, α-helical structural elements within the voltage-sensing domains of a K^+ channel. *J. Gen. Physiol.* **115**, 33–50 (2000).
29. A. Cha, G. E. Snyder, P. R. Selvin, F. Bezanilla, Atomic scale movement of the voltage-sensing region in a potassium channel measured via spectroscopy. *Nature* **402**, 809–813 (1999).
30. S. I. Börjesson, S. Hammarström, F. Elinder, Lipoelectric modification of ion channel voltage gating by polyunsaturated fatty acids. *Biophys. J.* **95**, 2242–2253 (2008).
31. G. Adam, M. Delbrück, Reduction of dimensionality in biological diffusion processes, in *Structural and Molecular Biology* (Freeman, 1968).
32. A. Kamb, L. E. Iverson, M. A. Tanouye, Molecular characterization of Shaker, a *Drosophila* gene that encodes a potassium channel. *Cell* **50**, 405–413 (1987).
33. T. Hoshi, W. N. Zagotta, R. W. Aldrich, Biophysical and molecular mechanisms of Shaker potassium channel inactivation. *Science* **250**, 533–538 (1990).
34. S. I. Börjesson, T. Parkkari, S. Hammarström, F. Elinder, Electrostatic tuning of cellular excitability. *Biophys. J.* **98**, 396–403 (2010).
35. B. Frankenhaeuser, Potassium permeability in myelinated nerve fibres of *Xenopus laevis*. *J. Physiol.* **160**, 54–61 (1962).
36. B. Hille, *Ion Channels of Excitable Membranes* (Sinauer, 2001), vol. 507.
37. X.-p. Xu, D. Erichsen, S. I. Börjesson, M. Dahlin, P. Åmark, F. Elinder, Polyunsaturated fatty acids and cerebrospinal fluid from children on the ketogenic diet open a voltage-gated K channel: A putative mechanism of antiseizure action. *Epilepsy Res.* **80**, 57–66 (2008).
38. D. M. Lorber, B. K. Shoichet, Hierarchical docking of databases of multiple ligand conformations. *Curr. Top. Med. Chem.* **5**, 739–749 (2005).
39. B. K. Shoichet, I. D. Kuntz, Matching chemistry and shape in molecular docking. *Protein Eng.* **6**, 723–732 (1993).
40. A. Nicholls, B. Honig, A rapid finite difference algorithm, utilizing successive over-relaxation to solve the Poisson–Boltzmann equation. *J. Comput. Chem.* **12**, 435–445 (1991).
41. S. J. Weiner, P. A. Kollman, D. A. Case, U. C. Singh, C. Ghio, G. Alagona, S. Profeta, P. Weiner, A new force field for molecular mechanical simulation of nucleic acids and proteins. *J. Am. Chem. Soc.* **106**, 765–784 (1984).
42. E. C. Meng, B. K. Shoichet, I. D. Kuntz, Automated docking with grid-based energy evaluation. *J. Comput. Chem.* **13**, 505–524 (1992).
43. J. J. Irwin, T. Sterling, M. M. Mysinger, E. S. Bolstad, R. G. Coleman, ZINC: A free tool to discover chemistry for biology. *J. Chem. Inf. Model.* **52**, 1757–1768 (2012).
44. J. D. Yesselman, D. J. Price, J. L. Knight, C. L. Brooks III, MATCH: An atom-typing toolset for molecular mechanics force fields. *J. Comput. Chem.* **33**, 189–202 (2012).
45. D. Van Der Spoel, E. Lindahl, B. Hess, G. Groenhof, A. E. Mark, H. J. C. Berendsen, GROMACS: Fast, flexible, and free. *J. Comput. Chem.* **26**, 1701–1718 (2005).
46. S. Pronk, S. Páll, R. Schulz, P. Larsson, P. Bjelkmar, R. Apostolov, M. R. Shirts, J. C. Smith, P. M. Kasson, D. van der Spoel, B. Hess, E. Lindahl, GROMACS 4.5: A high-throughput and highly parallel open source molecular simulation toolkit. *Bioinformatics* **29**, 845–854 (2013).
47. S. Miller, J. Janin, A. M. Lesk, C. Chothia, Interior and surface of monomeric proteins. *J. Mol. Biol.* **196**, 641–656 (1987).
48. Y.-M. Cui, E. Yasutomi, Y. Otani, T. Yoshinaga, K. Ido, K. Sawada, T. Ohwada, Novel BK channel openers containing dehydroabietic acid skeleton: Structure-activity relationship for peripheral substituents on ring C. *Bioorg. Med. Chem. Lett.* **18**, 5201–5205 (2008).
49. C.-K. Lee, J.-M. Fang, Y.-s. Cheng, Abietanes from leaves of Juniperus chinensis. *Phytochemistry* **35**, 983–986 (1994).
50. M. G. Organ, S. Çalimsiz, M. Sayah, K. H. Hoi, A. J. Lough, Pd-PEPPSI-IPent: An active, sterically demanding cross-coupling catalyst and its application in the synthesis of tetra-ortho-substituted biaryls. *Angew. Chem. Int. Ed. Engl.* **48**, 2383–2387 (2009).
51. A. Presser, E. Haslinger, R. Weis, A. Hüfner, Synthetic transformations of abietic acid IV [1]. B- and C-ring oxidation. *Monatshefte für Chemie* **129**, 921–930 (1998).

Acknowledgments: We thank A. Ranganathan and J. Carlsson for help with initial docking and ligand parameters and G. von Heine, P. Larsson, and S. Liin for comments on the manuscript. **Funding:** This work was supported by grants from the Swedish Research Council, the Swedish Brain Foundation, the Swedish Heart-Lung Foundation, and the Swedish National Infrastructure for Computing. **Author contributions:** N.E.O., M.S.E., X.W., S.Y., P.K., E.L., and F.E. designed the experiments and analyzed the data. N.E.O. and M.S.E. performed the electrophysiological experiments. X.W. performed the chemical synthesis. S.Y. performed the molecular docking and dynamics simulations. N.E.O., M.S.E., X.W., S.Y., P.K., E.L., and F.E. wrote the paper. **Competing interests:** F.E., P.K., N.E.O., and X.W. are authors on a patent application related to this work (publication no. WO/2016/114707, application no. PCT/SE2016/050008, filed on 11 January 2016). The authors declare no other competing interests. **Data and materials availability:** All data needed to evaluate the conclusions in the paper are present in the paper and/or the Supplementary Materials. Additional data related to this paper may be requested from the authors.

Submitted 7 April 2017
Accepted 27 September 2017
Published 25 October 2017
10.1126/sciadv.1701099

Citation: N. E. Ottosson, M. Silverå Ejneby, X. Wu, S. Yazdi, P. Konradsson, E. Lindahl, F. Elinder, A drug pocket at the lipid bilayer–potassium channel interface. *Sci. Adv.* **3**, e1701099 (2017).